Polarization Effect of a Dielectric Membrane on the Ionic Current Rectification in a Conical Nanopore

ARTICLE *in* THE JOURNAL OF PHYSICAL CHEMISTRY C · DECEMBER 2011

Impact Factor: 4.77 · DOI: 10.1021/jp2089388

THE JOURNAL OF PHYSICAL CHEMISTRY C

ARTICLE

pubs.acs.org/JPCC

Polarization Effect of a Dielectric Membrane on the Ionic Current Rectification in a Conical Nanopore

Bingkai Zhang,[†] Ye Ai,[‡] Jing Liu,[*,†] Sang W. Joo,[§] and Shizhi Qian[*,‡,§]

[†]State Key Laboratory of Coal Combustion, Huazhong University of Science and Technology, Wuhan 430074, China

[‡]Institute of Micro/Nanotechnology, Old Dominion University, Norfolk, Virginia 23529, United States

[§]School of Mechanical Engineering, Yeungnam University, Gyongsan 712-749, South Korea

ABSTRACT: Ionic current rectification (ICR) refers to a phenomenon that an ionic current flowing through a nanopore exhibits a preferential direction. In this paper, we investigate the ICR phenomenon in a conical nanopore embedded within a dielectric membrane using a continuum-based model, which is composed of the Nernst−Planck (NP) equations for the ionic mass transport, the Poisson equation for the electrostatics, and the Navier−Stokes (NS) equations for the flow field. Different from the existing studies, the emphasis of this investigation is placed on the polarization effect of the dielectric membrane on the ionic current and ICR in a conical nanopore. The results show that the polarization effect can influence the ion current and ICR, especially under the conditions of a relatively low κR_t, which is the ratio of the nanopore tip radius and the Debye length, and a relatively low surface charge density of the nanopore.

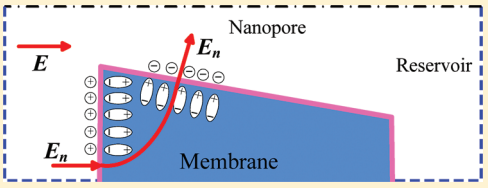

1. INTRODUCTION

In recent years, there has been a growing interest in the development of lab-on-a-chip devices using synthetic nanopores as a new tool for drug delivery, sensing, and manipulation of biomolecules such as DNA.[1−5] This conception is inspired by nature, in that biological ionic channels are the basis of many physiological processes in a living organism. Several interesting ion transport phenomena, such as ionic current rectification (ICR)[6−12] and ionic selectivity,[11,13−16] have been observed in conical nanopores. A comprehensive understanding of ion transport in synthetic nanopores not only increases our knowledge of physiological processes in biological ionic channels, but also facilitates the development of practical nanofluidic devices for various biomedical applications.

ICR in conical nanopores implies a preferential direction of the ionic current through the nanopores, resulting in an asymmetric diode-like current−voltage (I−V) behavior. The ICR phenomenon has been widely investigated theoretically and experimentally in various nanofluidic channels, such as silica nanochannels,[17] porous glass membranes[18] and track-etched polymer pores. These studies have found that the ICR could be influenced by many factors, such as the salt concentration gradient,[19] the pore size[20] and the surface charge density distribution.[21] The existing studies further demonstrated that the asymmetric distribution of the surface charge density along the nanopore is responsible for the ICR phenomenon.[11,12,22−26] The modification of the surface charge can be achieved by controlling the pH value of the aqueous solution,[27,28] special chemical treatment,[17,29] and field effect transistor.[21,30] The control of the surface charge leads to a more sophisticated modulation of the ICR in conical nanopores, which could be a starting point of more complex nanofluidic ionic devices.

When a dielectric material is subjected to an external electric field, as shown in Figure 1a, electric charges do not flow through the material, which is different from a conductor. However, polarization of atoms or molecules of the dielectric material produces an electric field within the dielectric material that partially compensates the external electric field. In addition, the polarization effect induces charges on the surface of the dielectric material, as shown in Figure 1b,c. Synthetic nanopores are typically fabricated using dielectric materials such as silicon dioxide, polymers, and proteins. Thus, the polarization charge induced at the interface between the fluid and the dielectric material would affect the ICR arising from the electrostatic interaction between asymmetrically distributed surface charge and mobile ions.[11,12,23−26] Recently, the polarization effect of protein membrane on the ionic selectivity in a calcium channel has been investigated by Boda et al.[31] It has been found that a lower relative permittivity of the protein membrane could attract more cations into the nanopore due to the negative charge induced on the dielectric surface by the protein's carboxyl groups. In addition, the induced charge on a dielectric tip in a microchannel could generate vortex due to the polarization effect, referring to the induced charge electroosmosis, which has been experimentally observed[32,33] and numerically predicted.[32] So far, theoretical and experimental investigations of the polarization effect on the ICR in conical nanopores have not been reported.

In this paper, we conduct the first theoretical study of the polarization effect on the ICR in a conical nanopore embedded within a dielectric membrane. The numerical results are obtained

Received: September 15, 2011
Revised: November 9, 2011
Published: November 09, 2011

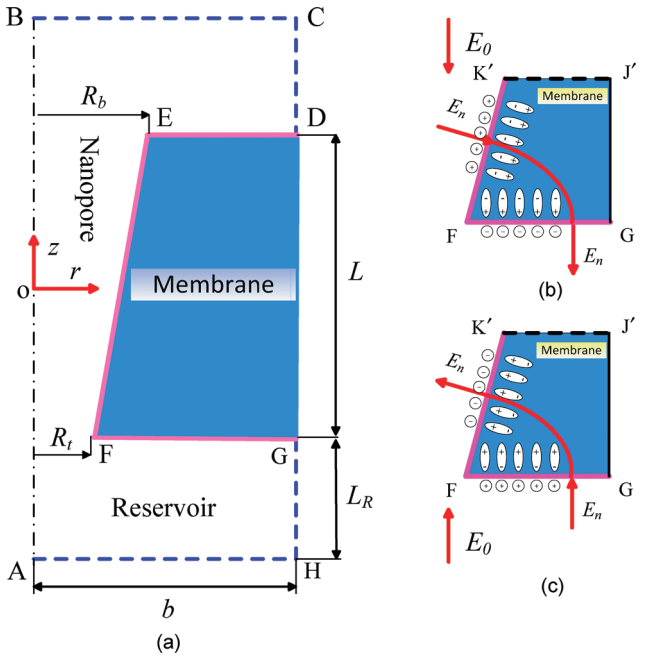

Figure 1. (a) A charged conical nanopore embedded within a solid dielectric membrane connects two identical reservoirs filled with a binary electrolyte solution. An electric field imposed parallel to the axis of the nanopore generates an ionic current through the conical nanopore. Negative (b) and positive (c) external electric fields lead to opposite polarizations of the dielectric membrane. Polarization charges are induced on the surface of the dielectric membrane. Note that segment K′J′ is the interior of the dielectric membrane.

by solving a verified continuum-based model, which is composed of the Poisson−Nernst−Planck (PNP) equations and the Navier−Stokes (NS) equations. It has been demonstrated that the adopted continuum-based model is still valid to predict the ion transport in nanopores when the pore radius is larger than one Debye length.[34−36] In addition, the effects due to the imposed voltage bias, the ratio of the tip size to the Debye length, the inherent surface charge density of the nanopore on the polarization of the dielectric membrane, and the resulting ICR have also been investigated.

2. MATHEMATICAL MODEL

Figure 1a depicts a conical nanopore embedded within a dielectric membrane with relative permittivity ε_m connecting two identical reservoirs on either side. The computational domain includes the fluid domain Ω_f and the membrane domain Ω_m, which are, respectively, enclosed by segments ABCDEFGH and DEFG. The axial length of the nanopore and the radii of the nanopore's tip and base are, respectively, L, R_t, and R_b. The length L_R and radius b of the reservoirs are sufficiently large to ensure the numerical results are independent of the reservoir size. The two reservoirs are filled with a binary KCl electrolyte solution at the bulk ionic concentration C_0 with density ρ, dynamic viscosity μ, and relative permittivity ε_f. The origin of the cylindrical coordinate (r, z) is located at the center of the nanopore. The surface of the nanopore (segment EF) and the wall of the reservoirs (segments DE and FG) inherently bear a uniform surface charge density σ. An electric potential difference V is applied between the bottom (segment AH) and upper (segment BC) reservoirs to generate the ionic current and also electroosmotic flow (EOF) through the nanopore.

2.1. Mathematical Model for Fluid Motion. Recent studies revealed that the EOF could significantly affect the ICR when the surface charge of the nanopore is very high.[37] Therefore, the EOF and the resulting convective ion transport are taken into account in the present study. As the Reynolds number is usually very small in nanofluidics, the inertial terms in the NS equations can be safely neglected. The conservation of mass requires

$$\nabla \cdot \mathbf{u} = 0 \text{ in } \Omega_f \tag{1}$$

and the conservation of momentum is given by

$$-\nabla p + \mu \nabla^2 \mathbf{u} - \rho_e \nabla \varphi = 0 \text{ in } \Omega_f \tag{2}$$

In the above, $\mathbf{u}$ is the fluid velocity; p is the pressure; ϕ is the electric potential; and $\rho_e = F\sum_{i=1}^{n} z_i c_i$ is the space charge density, where F is the Faraday constant, z_i is the valence of the ith ionic species, c_i is the ionic concentration of the ith ionic species, and n is the total number of ionic species in the electrolyte solution. The last term on the left-hand side of eq 2 is the electrostatic body force acting on the fluid arising from the electrostatic interaction between the net charge density of the electrolyte solution and the applied electric field.

The boundary conditions for the fluid motion are given as follows: On the walls of the two reservoirs (segments DE and FG) and the surface of the nanopore (segment EF) in Figure 1a, the velocity satisfies the no slip condition. The axial symmetry boundary condition is used along segment AB. Normal flow with $p = 0$ is imposed on segments AH and BC. Finally, slip boundary conditions are imposed on segments CD and FG, which are far away from the nanopore.

2.2. Mathematical Model for Ionic Mass Transport. To obtain the electrostatic force required to solve eq 2, the electric potential and the ionic distribution within the electrolyte solution need to be solved. In addition, the electric potential within the dielectric membrane is also solved to address the polarization of the membrane and the induced surface charge along the nanopore's surface. The distributions of the electric potential within the fluid and the membrane are, respectively, governed by the Poisson equation

$$-\varepsilon_0 \varepsilon_f \nabla^2 \varphi = \rho_f \text{ in } \Omega_f \tag{3}$$

and the Laplace equation

$$\nabla^2 \psi = 0 \text{ in } \Omega_m \tag{4}$$

Here, ε_0 is the absolute permittivity of a vacuum, and ψ is the electric potential within the dielectric membrane.

The electric potentials applied on segments AH and BC are, respectively,

$$\varphi_{AH} = V \text{ and } \varphi_{BC} = 0 \tag{5}$$

When V is positive, the imposed electric field is directed from the tip toward the base of the nanopore, and vice versa. Surface charge boundary condition applied on the surface of the nanopore (segment EF) and the walls of the reservoirs (segments DE and FG) is given by

$$\mathbf{n} \cdot (-\varepsilon_0 \varepsilon_f \nabla \varphi) + \mathbf{n} \cdot (\varepsilon_0 \varepsilon_m \nabla \psi) = \sigma \tag{6}$$

where $\mathbf{n}$ is the unit normal vector pointed from the boundary into the fluid. In addition, the electric potential at the membrane/fluid interface is continuous, $\phi = \psi$. Normal electric field on segments

CD, DG, and GH is zero, and axial symmetry boundary condition is imposed on segment AB.

The ionic flux within the KCl electrolyte solution arising from convection, diffusion, and electromigration is given by

$$\mathbf{N}_i = \mathbf{u}c_i - D_i\nabla c_i - z_i\frac{D_i}{RT}Fc_i\nabla\varphi, \quad i = 1 \text{ and } 2 \tag{7}$$

where D_i is the diffusivity of the ith ionic species, R is the universal gas constant, and T is the absolute temperature of the electrolyte solution. The mass conservation of each ionic species at a steady state satisfies the Nernst−Planck (NP) equation

$$\nabla\cdot\mathbf{N}_i = 0, \quad i = 1 \text{ and } 2 \tag{8}$$

Segments DE, EF, and FG are the walls of the reservoirs and the nanopore, which are impermeable to ions. Therefore, the normal ionic flux on these boundaries is zero, written as

$$\mathbf{n}\cdot\mathbf{N}_i = 0, \quad i = 1 \text{ and } 2 \tag{9}$$

As segments AH and BC are far away from the nanopore, the ionic concentrations at the two boundaries are the bulk value:

$$c_{i,\mathrm{AH}} = c_{i,\mathrm{BC}} = C_0, \quad i = 1 \text{ and } 2 \tag{10}$$

Axial symmetry boundary condition is imposed on AB, and zero normal ionic flux is applied along CD and GH since they are in the bulk electrolyte reservoirs.

The ionic current through the nanopore can be calculated by the following expression:

$$I = \int_S F\sum(z_i\mathbf{N}_i)\cdot\mathbf{n}\,dS, \quad i = 1 \text{ and } 2 \tag{11}$$

where S is the cross-sectional area of the nanopore.

We normalize the above governing equations by choosing the bulk concentration C_0 as the ionic concentration scale, RT/F as the potential scale, the tip radius R_t as the length scale, $U_0 = \varepsilon_0\varepsilon_f R^2T^2/(\mu R_t F^2)$ as the velocity scale, and $\mu U_0/R_t$ as the pressure scale. The dimensionless governing equations 1, 2, 3, 4, and 8 are thus obtained:

$$\nabla^*\cdot\mathbf{u}^* = 0 \tag{12}$$

$$-\nabla^* p^* + \nabla^{*2}\mathbf{u}^* - \frac{1}{2}(\kappa R_t)^2(z_1c_1^* + z_2c_2^*)\nabla\varphi^* = 0 \tag{13}$$

$$-\nabla^{*2}\varphi^* = \frac{1}{2}(\kappa R_t)^2(z_1c_1^* + z_2c_2^*) \tag{14}$$

$$\nabla^{*2}\psi^* = 0 \tag{15}$$

$$\nabla^*\cdot\mathbf{N}_i^* = 0, \quad i = 1 \text{ and } 2 \tag{16}$$

Hereafter, all variables with a superscript asterisk are dimensionless. $\kappa^{-1} = \lambda_D = (\varepsilon_0\varepsilon_f RT/2F^2C_0)^{1/2}$ is the Debye length. The dimensionless flux density normalized by U_0C_0 is

$$\mathbf{N}_i^* = \mathbf{u}^*c_i^* - \Lambda_i\nabla^*c_i^* - z_i^*\Lambda_ic_i^*\nabla^*\varphi^*, \quad i = 1 \text{ and } 2 \tag{17}$$

where $\Lambda_i = D_i/D_0$ with $D_0 = \varepsilon_0\varepsilon_f R^2T^2/(\mu F^2)$. The surface charge boundary condition normalized by $\varepsilon_0\varepsilon_f RT/(FR_t)$ is

$$\mathbf{n}\cdot(-\nabla^*\varphi^*) + \mathbf{n}\cdot\left(-\frac{\varepsilon_m}{\varepsilon_f}\nabla^*\psi^*\right) = \sigma^* \tag{18}$$

The dimensionless ionic current through the nanopore normalized with $FU_0C_0R_t^2$ is

$$I^* = \int\sum(z_i^*\mathbf{N}_i^*)\cdot\mathbf{n}\,dS^*, \quad i = 1 \text{ and } 2 \tag{19}$$

The strongly coupled PNP and NS equations are solved by a commercial finite-element package COMSOL (version 3.5a, www.comsol.com) operating in a high performance cluster. The accuracy of the finite-element package has been carefully examined in previous studies.[38−45] In the present study, the computational domain, as schematically shown in Figure 1a, is discretized into quadratic triangular elements. The main reason to choose the triangular mesh over the quadrilateral mesh in the current work is because the former one is easier to be generated in COMSOL. Typically, the total number of elements is about 6×10^5, and the relative error tolerance is 1×10^{-6}. Finer mesh is generated in the region close to the tip of the nanopore where the electrical double layer (EDL) may overlap. All the above settings guarantee the numerical results are accurate, converged, and grid-independent. In general, it takes about 3 h to complete one single simulation.

3. RESULTS AND DISCUSSION

In this section, we focus on the polarization effect of the dielectric membrane on the ICR in a conical nanopore. In the following simulations, the relative permittivity of aqueous solution KCl is $\varepsilon_f = 80$; the diffusion coefficients of K^+ and Cl^- are, respectively, $D(K^+) = 1.95 \times 10^{-9}$ m^2/s and $D(Cl^-) = 2.03 \times 10^{-9}$ m^2/s; the temperature of the system is $T = 300$ K; and the fluid density and viscosity are, respectively, $\rho = 1 \times 10^3$ kg/m^3 and $\mu = 1 \times 10^{-3}$ Pa·s. The dimensions of the nanopore are $R_t = 10$ nm, $R_b = 60$ nm and $L = 1$ μm. The radius and the length of each reservoir are $b = L_R = 0.4$ μm, which are confirmed to be large enough to eliminate the size effect of the reservoir. The resulting dimensionless ionic current through the nanopore is investigated as functions of the imposed dimensionless voltage, $\overline{V}$, the ratio of the tip size to the Debye length, κR_t, the relative permittivity of the membrane, ε_m, and the dimensionless surface charge density of the nanopore, σ^*.

The conical nanopore could be made of many dielectric materials, for example, proteins that have a relative permittivity between 2 and 80.[31,46−49] It has been found that the interior of proteins has a uniform high relative permittivity due to polarization contributions from the configurational freedom of polar side chains, which is in good agreement with experimental titration results.[50,51] In this study, the relative permittivity of the membrane, ε_m, ranges from 0 to 80, in which $\varepsilon_m = 0$ implies that the polarization effect of the membrane is not considered. The results show that the change in the relative permittivity of the membrane could lead to distinct ionic selectivity in the conical nanopore.

3.1. Effect of the Relative Permittivity of Dielectric Membrane, ε_m. Figures 2 and 3 depict, respectively, the dimensionless $I-V$ curves in a conical nanopore for $\kappa R_t = 1$ and 3 when the inherent surface charge densities of the nanopore are $\sigma^* = -2.73$ (a),

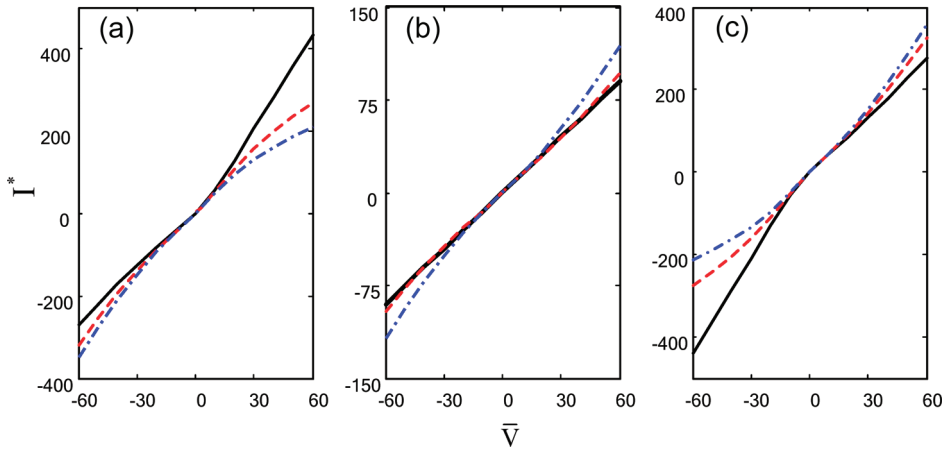

Figure 2. $I-V$ curves in a conical nanopore when $\sigma^* = -2.73$ (a), 0 (b), and 2.73 (c). Solid, dashed, and dash-dotted lines represent, respectively, $\varepsilon_m = 0$, 40, and 80 when $\kappa R_t = 1$.

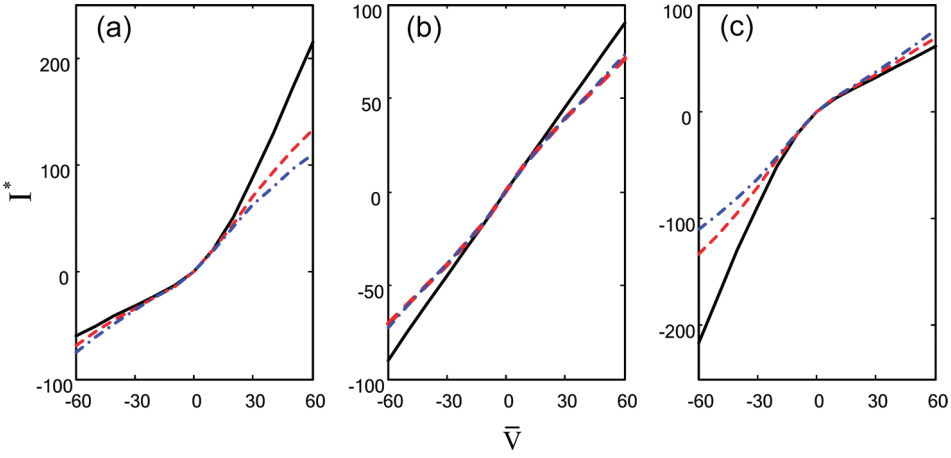

Figure 3. $I-V$ curves in a conical nanopore when $\sigma^* = -2.73$ (a), 0 (b), and 2.73 (c). Solid, dashed, and dash-dotted lines represent, respectively, $\varepsilon_m = 0$, 40, and 80 when $\kappa R_t = 3$.

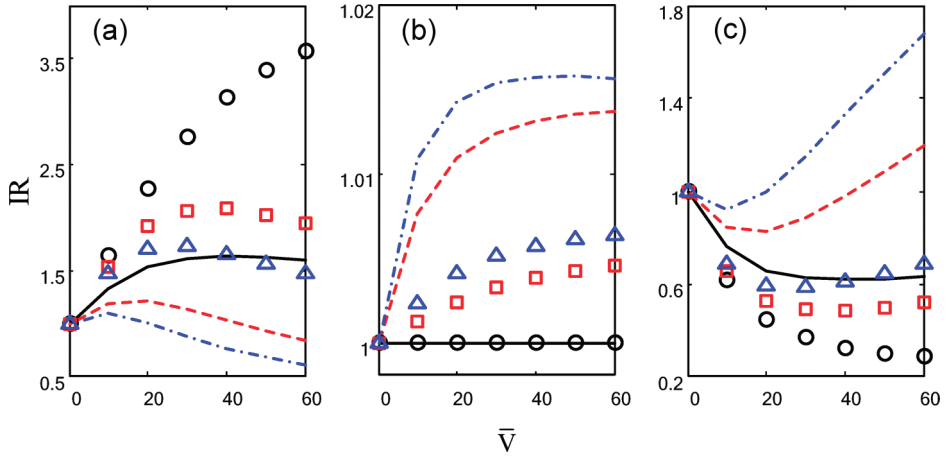

Figure 4. Current rectification ratio, IR, as a function of the applied voltage bias when $\sigma^* = -2.73$ (a), 0 (b) and 2.73 (c). Solid (circles), dashed (squares), and dash-dotted lines (triangles) represent, respectively, $\varepsilon_m = 0$, 40, and 80 when $\kappa R_t = 1$ ($\kappa R_t = 3$).

0 (b) and 2.73 (c). Solid lines, dashed lines, and dash-dotted lines are, respectively, the numerical results with the relative permittivity of the membrane, $\varepsilon_m = 0$, 40, and 80. In these simulations, the base side (segment BC) is grounded, while the

dx.doi.org/10.1021/jp2089388 |J. Phys. Chem. C 2011, 115, 24951–24959

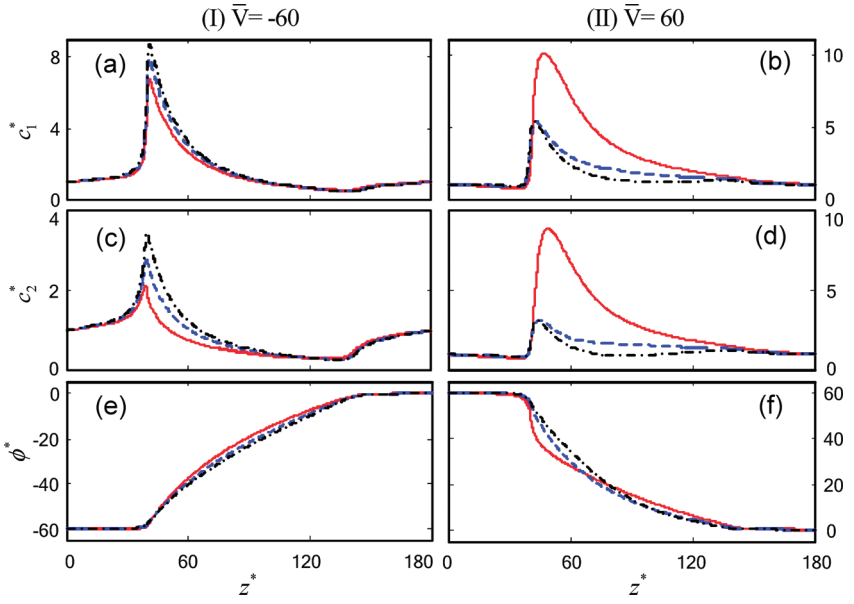

Figure 5. Cross-sectional averaged ionic concentrations and potential for $\overline{V} = -60$ (I) and 60 (II) along the nanopore when $\kappa R_t = 1$ and $\sigma^* = -2.73$. Solid, dashed, and dash-dotted lines represent, respectively, $\varepsilon_m = 0$, 40, and 80.

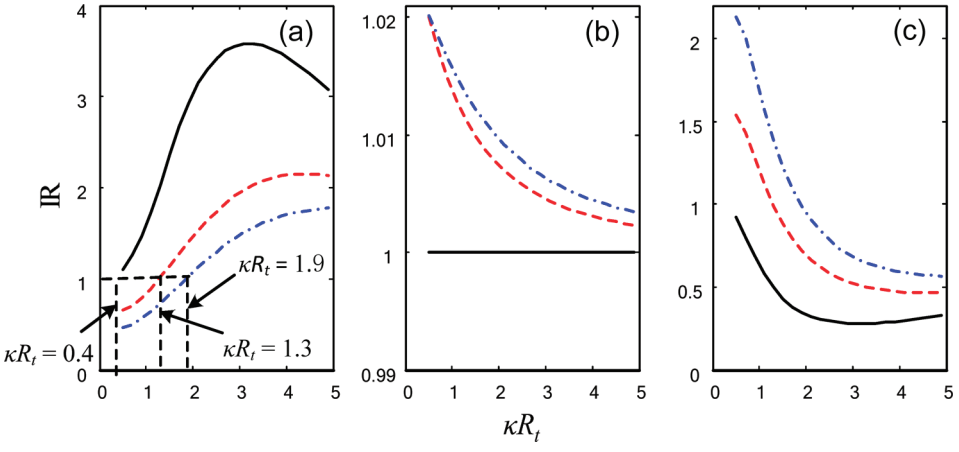

Figure 6. Current rectification ratio, *IR*, as a function of κR_t when $|\overline{V}| = 60$, $\sigma^* = -2.73$ (a), 0 (b), and 2.73 (c). Solid, dashed, and dash-dotted lines represent, respectively, $\varepsilon_m = 0$, 40, and 80.

dimensionless potential at the tip side (segment AH) varies from −60 to 60. The positive ionic current is defined as a current directed from the tip toward the base when a positive voltage bias ($V = \phi_{AH} - \phi_{BC} > 0$) is applied. The two figures reveal that the ionic current increases nonlinearly with the voltage bias when the nanopore carries a surface charge, indicating the diode-like *I*−*V* behavior in the conical nanopore. When the nanopore is neutral, as shown in Figures 2b and 3b, the ionic current is linearly proportional to the applied voltage. Apparently, the diode-like *I*−*V* behavior originates from the surface charge of the nanopore. A comparison of the *I*−*V* curves between the two different κR_t values (Figures 2 and 3) demonstrates that the magnitude of ionic current and the degree of ICR are both affected by κR_t. In addition, the relative permittivity of the dielectric membrane could also significantly affect the *I*−*V* curve. When $\kappa R_t = 3$, a higher relative permittivity of the dielectric membrane can dramatically suppress the ICR. When the inherent surface charge of the nanopore is reversed, the ICR is accordingly reversed.

Figure 4 depicts the current rectification ratio, $IR = |I(V)/I(-V)|$, as a function of the magnitude of the applied voltage bias. The *IR*−*V* curves under different ε_m values for $\kappa R_t = 1$ and 3 show a similar tendency. When the nanopore carries a negative surface charge, as shown in Figure 4a, the preferential ICR direction is directed from the tip toward the base without considering the polarization effect of the membrane (i.e., $\varepsilon_m = 0$). As the relative permittivity of the dielectric membrane increases, the preferential ICR direction could be reversed when $\kappa R_t = 1$. By contrast, the preferential ICR direction is unchanged when $\kappa R_t = 3$. However, the current rectification ratio, *IR*, is significantly reduced as the relative permittivity of the dielectric membrane increases. The relative difference of the current rectification ratio between $\varepsilon_m = 0$ and $\varepsilon_m = 80$ is 62.3% (58.6%) when $\overline{V} = 60$ and $\kappa R_t = 1$ ($\kappa R_t = 3$). When $\kappa R_t = 3$, a higher voltage bias usually leads to a higher current rectification ratio if $\varepsilon_m = 0$. When the relative permittivity of the dielectric membrane is relatively high, the polarization effect of the

dx.doi.org/10.1021/jp2089388 |*J. Phys. Chem. C* 2011, 115, 24951–24959

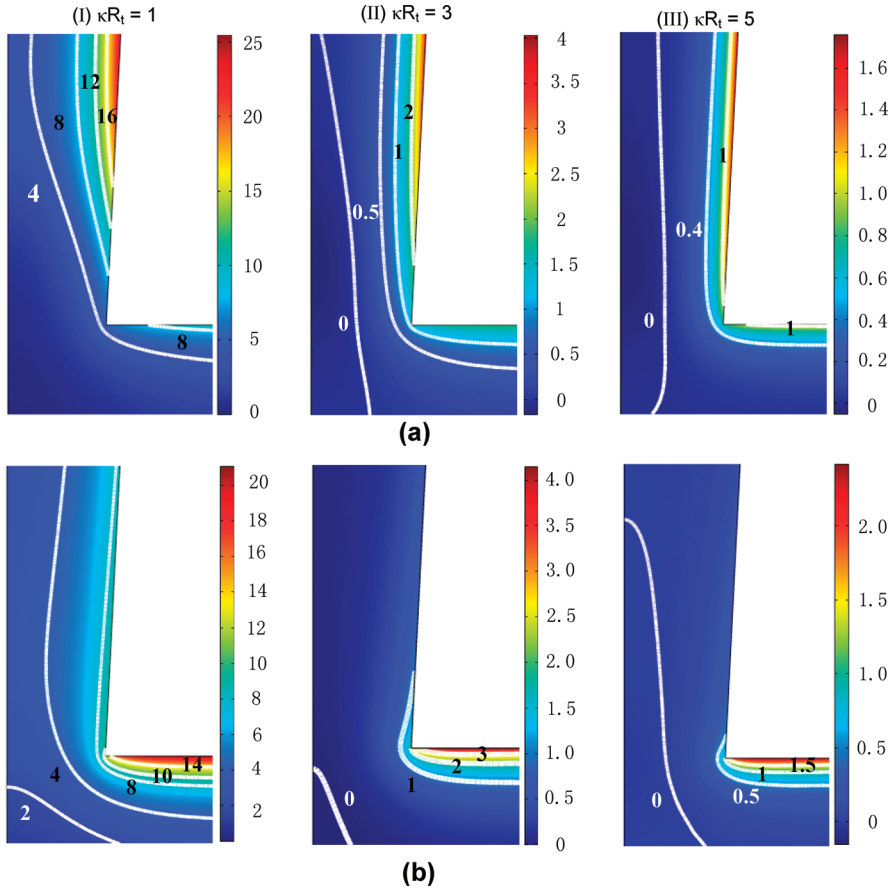

Figure 7. Distribution of the dimensionless ionic concentration difference between cation (K^+) and anion (Cl^-) near the tip of the conical nanopore when κR_t = 1 (I), 3 (II), and 5 (III) and ε_m = 0 (a), ε_m = 80 (b). σ^* = −2.73 and $\overline{V}$ = 60.

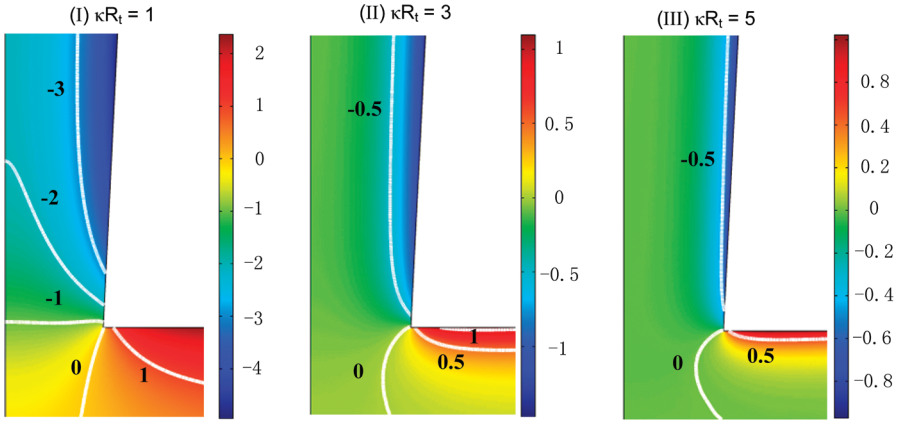

Figure 8. Distribution of the dimensionless ionic concentration difference between cation (K^+) and anion (Cl^-) near the tip of the conical nanopore when κR_t = 1 (I), 3 (II), and 5 (III). ε_m = 80, σ^* = 0, and $\overline{V}$ = 60.

membrane also becomes more pronounced as the applied voltage bias increases. As pointed out previously, the polarization effect tends to suppress the ICR. Therefore, the current rectification ratio is maximized at an intermediate voltage bias. When the nanopore is neutral, the ICR vanishes if ε_m = 0. As the relative permittivity of the dielectric membrane increases, a slight ICR is observed owing to the induced surface charge along the nanopore arising from the polarization effect. When the nanopore carries the same magnitude of surface charge as Figure 4a, however, with an opposite polarity, the ICR is reversed, as shown in Figure 4c.

To further explain the polarization effect of the membrane on the ICR in the conical nanopore, the cross-sectional averaged ionic concentrations and electric potential along the axis of the conical nanopore when κR_t = 1 and σ^* = −2.73 is shown in Figure 5. The cross-sectional averaged ionic concentration is

dx.doi.org/10.1021/jp2089388 |J. Phys. Chem. C 2011, 115, 24951–24959

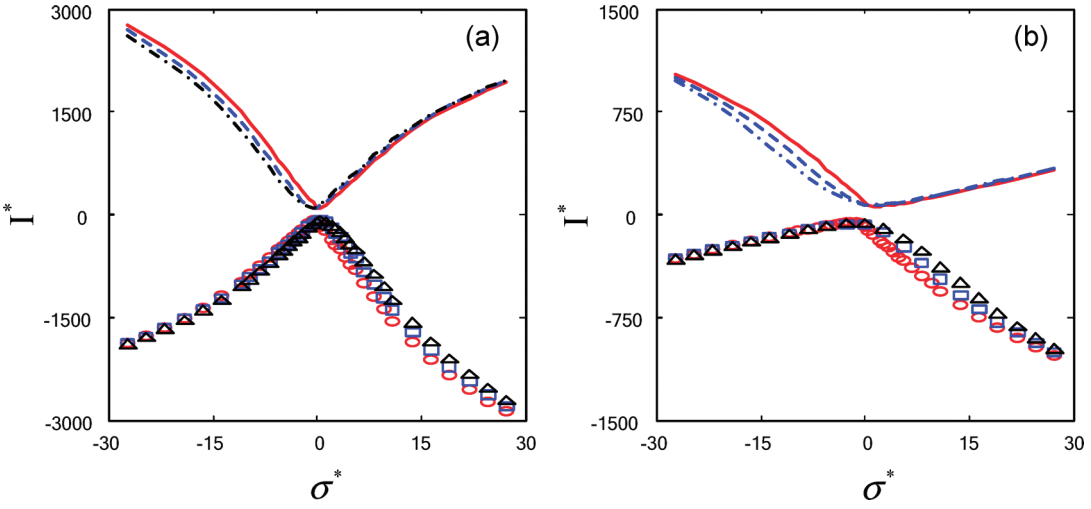

Figure 9. Ionic current as a function of the inherent surface charge density of the nanopore when $\kappa R_t = 1$ (a) and 3 (b). Solid (circles), dashed (squares), and dash-dotted lines (triangles) represent, respectively, $\varepsilon_m = 0$, 40, and 80 when $\overline{V} = 60$ ($\overline{V} = -60$).

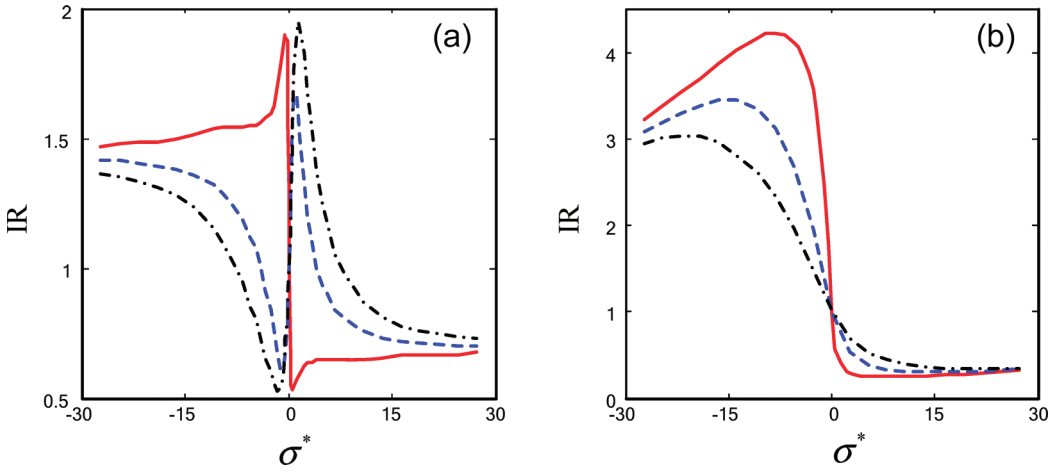

Figure 10. Current rectification ratio, *IR*, as a function of the inherent surface charge density of the nanopore when $\overline{V} = 60$, $\kappa R_t = 1$ (a) and 3 (b). Solid, dashed, and dashed-ditted lines represent, respectively, $\varepsilon_m = 0$, 40, and 80.

defined as the integration of ionic concentration over the cross-section divided by the cross-sectional area. When $\varepsilon_m = 0$, ion depletion is predicted in most region of the nanopore, while ion enrichment is only observed in the tip region of the nanopore when a negative voltage bias is applied along the nanopore (solid lines in Figure 5I). In contrast, ion enrichment is predicted along the entire nanopore when a positive voltage bias is applied (solid lines in Figure 5II). Ion depletion (enrichment) accordingly decreases (increases) the electrical conductance of the nanopore, which in turn leads to a lower (higher) ionic current flowing through the nanopore. This is the main mechanism of ICR, which has also been predicted in previous studies.[19,39] When the polarization effect of the membrane is taken into account, the cross-sectional averaged ionic concentrations and electric potential are accordingly altered. When a negative voltage is applied, the ion enrichment near the tip region is slightly enhanced. However, the cross-sectional averaged ionic concentration in the other region nearly remains unchanged compared to the case of $\varepsilon_m = 0$. In addition, the response of the cross-sectional averaged electric potential to the change in the relative permittivity of the membrane is very limited. Therefore, the ionic current is slightly enhanced under a negative voltage bias when considering the polarization effect, as indicated in Figure 2a. When a positive voltage bias is applied, the ion enrichment is significantly suppressed along the entire nanopore, as shown in Figure 5II. Consequently, the ionic current under a positive voltage bias is reduced, as shown in Figure 2a. The ICR for $\kappa R_t = 3$ is similar to that for $\kappa R_t = 1$, and thus is not discussed further.

3.2. Effect of the Ratio of the Tip Radius to the Debye Length, κR_t. Figure 6 shows the current rectification ratio as a function of κR_t under three different relative permittivities of the membrane. When the nanopore carries a negative surface charge and $\varepsilon_m = 0$, the current rectification ratio is maximized at an intermediate κR_t ($\kappa R_t \approx 3$ in the present study). This phenomenon has been experimentally observed by Schiedt et al.,[12] and also numerically predicted by White and Bund[38] and Ai et al.[39] recently. Although the polarization effect of the membrane suppresses the ICR, the effect of κR_t on the ICR for various ε_m is very similar. More interesting, it is found that there is a critical κR_t value at which the ICR in the conical nanopore vanishes.

dx.doi.org/10.1021/jp2089388 |J. Phys. Chem. C 2011, 115, 24951–24959

Beyond this critical κR_t, the preferential ionic current direction reverses. Figure 6a reveals that the critical ICR vanishing points for ε_m = 0, 40, and 80 are, respectively, κR_t = 0.4, 1.3, and 1.9. Apparently, a higher relative permittivity of the dielectric membrane leads to a higher critical κR_t value. When the nanopore is neutral and ε_m = 0, the ICR cannot be expected and is independent of κR_t, as shown in Figure 6b. Once the polarization effect is considered, a slight ICR is observed because of the induced surface charge along the nanopore. In addition, the polarization effect decreases as κR_t increases. The ICR in Figure 6c is the inversion of Figure 6a because the polarity of the surface charge is opposite.

To gain insight into the impact of κR_t on the polarization effect of the dielectric membrane, Figure 7 depicts the ionic concentration difference between cations and anions, $c_1^* - c_2^*$, near the tip region of the nanopore for κR_t = 1 (I), 3 (II), and 5 (III) when σ^* = −2.73, $\overline{V}$ = 60, ε_m = 0 (a) and ε_m = 80 (b). When κR_t = 1 and ε_m = 0 (Figure 7aI), cations are dominantly occupied inside the nanopore, resulting in a preferential ionic current direction. Once the polarization effect is taken into account, the ionic concentrations are significantly altered, as shown in Figure 7bI. As the applied voltage bias is positive, the tip of the nanopore is closer to the anode. Therefore, negative polarization charges are induced on the wall of the reservoir close to the anode (segment FG), which in turn attracts more cations, as shown in Figure 7bI. Oppositely, the enrichment of cations near the surface of the nanopore (segment EF) is diminished, which implies that positive polarization charges are induced on the surface of the nanopore. Therefore, the inherent surface charge of the nanopore is partially cancelled by the induced charge. As a result, the positive ionic current is suppressed by the polarization effect of the dielectric membrane, which agrees with the prediction in Figure 2a. When a negative voltage bias is applied, the induced surface charge along the nanopore is negative, which accordingly enhances the negative ionic current, as shown in Figure 2a. Obviously, the ionic concentration within one Debye length region could be significantly affected by the induced charged. When the bulk ionic concentration is increased to maintain κR_t = 3, the bulk region becomes larger, as shown in Figure 7aII. Figure 7bII also shows that negative and positive polarization charges are, respectively, induced on segments FG and EF when ε_m = 80. However, the effect of the induced charge on the ion redistribution and the resulting ionic current becomes weaker as κR_t increases, which is also revealed in Figure 7III.

As previously mentioned, the ICR vanishes when the nanopore is neutral and ε_m = 0. Therefore, the dimensionless ionic concentrations of both cations and anions in the entire fluid domain are unity. Figure 8 shows the ionic concentration difference between cations and anions, $c_1^* - c_2^*$, near the tip region of the nanopore when κR_t = 1 (I), 3 (II), and 5 (III), ε_m = 80, σ^* = 0, and $\overline{V}$ = 60. It is even more obvious that more cations are attracted near segment FG, while more anions are presented near segment EF when the polarization effect is taken into account. Because of the induced charge along the nanopore, a slight ICR phenomenon is observed as shown in Figure 6b. As κR_t increases, the polarization effect on the ICR decreases. Therefore, the current rectification ratio decreases as κR_t increases, as shown in Figure 6b.

3.3. Effect of the Nanopore's Surface Charge Density, σ^*. Figure 9 shows the ionic current as a function of the surface charge density of the nanopore (I^*−σ^*curves). Here, the dimensional surface charge density ranges from −0.1 C/m^2 to 0.1 C/m^2, which could be tuned by several techniques mentioned previously. It is found that the ionic current increases with the magnitude of surface charge density, which is consistent with previous studies.[28,29,39,52] The effect of the nanopore's surface charge density on the current rectification ratio, *IR*, is shown in Figure 10. When the nanopore is neutral, the current rectification ratio is *IR* = 1, indicating a negligible ICR. Therefore, the electrostatic interaction between the asymmetrically distributed surface charge and ions inside the nanopore is responsible for the ICR phenomenon. The ICR is maximized at an intermediate surface charge density. It has also found that the polarization effect becomes significant when the inherent surface charge of the nanopore is relatively low. When the inherent surface charge is relatively high, it always dominates over the induced surface charge, resulting in a limited polarization effect. Therefore, the ICR could be regulated by controlling the relative permittivity of the dielectric membrane.

4. CONCLUSIONS

In this paper, we investigate the asymmetrical conductance behavior in a conical nanopore embedded in a dielectric membrane. The numerical results have been obtained based on a continuum-based axisymmetric model, composed of the PNP equations and the NS equations. The numerically predicted diode-like $I-V$ characteristics in a conical nanopore is in qualitative agreement with the existing experiments. The quantitative differences between the simulations and the experiments can be attributed to the complex three-dimensional (3D) geometry of the synthetic nanopore, which was not duplicated in the numerical simulations.

Four main effects, including the applied voltage bias, the relative permittivity of the dielectric membrane, the ratio of the tip radius to the Debye length, and the inherent surface charge density of the nanopore on the ICR in a conical nanopore have been numerically studied. It has been found that the ICR is maximized at an intermediate κR_t and an intermediate surface charge density of the nanopore, which agrees with a previous study.[39] Usually, the polarization effect of the dielectric nanopore tends to suppress the preferential ionic current, which thus diminishes the ICR. In addition, the polarization effect becomes dominant at a relatively low inherent surface charge density of the nanopore and a relatively thick EDL. Therefore, the ICR in a conical nanopore could be tuned by controlling the relative permittivity of the dielectric membrane.

AUTHOR INFORMATION

Corresponding Author
*E-mail: liujing27@mail.hust.edu.cn (J.L.); sqian@odu.edu (S.Q.).

ACKNOWLEDGMENT

This work was supported by the World Class University Grant No. R32-2008-000-20082-0 of the Ministry of Education, Science and Technology of Korea; the Korea Institute of Machinery & Materials (KIMM); and the Program for New Century Excellent Talents in University (No. NCET-10-0412) (J.L.).

REFERENCES

(1) Kasianowicz, J. J.; Brandin, E.; Branton, D.; Deamer, D. W. *Proc. Natl. Acad. Sci. U.S.A.* **1996**, *93*, 13770–13773.

(2) Clarke, J.; Wu, H. C.; Jayasinghe, L.; Patel, A.; Reid, S.; Bayley, H. *Nat. Nanotechnol.* **2009**, *4*, 265–270.
(3) Meller, A.; Nivon, L.; Branton, D. *Phys. Rev. Lett.* **2001**, *86*, 3435–3438.
(4) Ai, Y.; Qian, S. *Electrophoresis* **2011**, *32*, 996–1005.
(5) Ai, Y.; Qian, S. *Phys. Chem. Chem. Phys.* **2011**, *13*, 4060–4071.
(6) Apel, P.; Korchev, Y. E.; Siwy, Z.; Spohr, R.; Yoshida, M. *Nucl. Instrum. Methods Phys. Res. B* **2001**, *184*, 337–346.
(7) Siwy, Z.; Gu, Y.; Spohr, H. A.; Baur, D.; Wolf-Reber, A.; Spohr, R.; Apel, P.; Korchev, Y. E. *Europhys. Lett.* **2002**, *60*, 349–355.
(8) Siwy, Z.; Apel, P.; Dobrev, D.; Neumann, R.; Spohr, R.; Trautmann, C.; Voss, K. *Nucl. Instrum. Methods Phys. Res. B* **2003**, *208*, 143–148.
(9) Siwy, Z.; Dobrev, D.; Neumann, R.; Trautmann, C.; Voss, K. *Appl. Phys. A: Mater. Sci. Process.* **2003**, *76*, 781–785.
(10) Siwy, Z.; Apel, P.; Baur, D.; Dobrev, D.; Korchev, Y. E.; Neumann, R.; Spohr, R.; Trautmann, C.; Voss, K. *Surf. Sci.* **2003**, *532*−*535*, 1061–1066.
(11) Siwy, Z.; Kosińska, I. D.; Fuliński, A.; Martin, C. R. *Phys. Rev. Lett.* **2005**, *94*, 048102.
(12) Schiedt, B.; Healy, K.; Morrison, A. P.; Neumann, R.; Siwy, Z. *Nucl. Instrum. Methods Phys. Res., Sect. B* **2005**, *236*, 109–116.
(13) Siwy, Z.; Fulinski, A. *Am. J. Phys.* **2004**, *72*, 567–574.
(14) Cervera, J.; Alcaraz, A.; Schiedt, B.; Neumann, R.; Ramirez, P. *J. Phys. Chem. C* **2007**, *111*, 12265–12273.
(15) Ramirez, P.; Gomez, V.; Cervera, J.; Schiedt, B.; Mafe., S. *J. Chem. Phys.* **2007**, *126*, 194703.
(16) Siwy, Z. *Adv. Funct. Mater.* **2006**, *16*, 735–746.
(17) Karnik, R.; Duan, C.; Castelino, K.; Daiguji, H.; Majumdar, A. *Nano Lett.* **2007**, *7*, 547–551.
(18) Zhang, B.; Zhang, Y.; White, H. S. *Anal. Chem.* **2004**, *76*, 6229–6238.
(19) Cheng, L. J.; Guo, L. J. *Nano Lett.* **2007**, *7*, 3165–3171.
(20) Kovarik, M. L.; Zhou, K.; Jacobson, S. C. *J. Phys. Chem. C* **2009**, *113*, 15960–15966.
(21) Ai, Y.; Liu, J.; Zhang, B.; Qian, S. *Sens. Actuators, B: Chem.* **2011**, *157*, 742–751.
(22) Siwy, Z.; Heins, E.; Harrell, C. C.; Kohli, P.; Martin, C. R. *J. Am. Chem. Soc.* **2004**, *126*, 10850–10851.
(23) Mara, A.; Siwy, Z.; Trautmann, C.; Wang, J.; Kamme, F. *Nano Lett.* **2004**, *4*, 497–501.
(24) Woermann, D. *Nucl. Instrum. Methods Phys. Res., Sect. B* **2002**, *194*, 458–462.
(25) Woermann, D. *Phys. Chem. Chem. Phys.* **2003**, *5*, 1853–1858.
(26) Woermann, D. *Phys. Chem. Chem. Phys.* **2004**, *6*, 3130–3132.
(27) Alcaraz, A.; Ramirez, P.; Garcia, E.; Gimenez, M. L.; Lopez, A.; Andrio, V. M.; Aguilella *J. Phys. Chem. B* **2006**, *110*, 21205–21209.
(28) Ali, M.; Ramirez, P.; Mafé, S.; Neumann, R.; Ensinger, W. *ACS Nano* **2009**, *3*, 603–608.
(29) He, Y.; Gillespie, D.; Boda, D.; Vlassiouk, I.; Eisenberg, R. S.; Siwy, Z. *J. Am. Chem. Soc.* **2009**, *131*, 5194–5202.
(30) Ai, Y.; Liu, J.; Zhang, B.; Qian, S. *Anal. Chem.* **2010**, *82*, 8217–8225.
(31) Boda, D.; Valiskó, M.; Eisenberg, B.; Nonner, W.; Henderson, D. J.; Gillespie, D. *J. Chem. Phys.* **2006**, *125*, 034901.
(32) Eckstein, Y.; Yossifon, G.; Seifert, A.; Miloh, T. *J. Colloid Interface Sci.* **2009**, *338*, 243–249.
(33) Chen, J. K.; Yang, R. *J. Microfluid. Nanofluid.* **2008**, *5*, 719–725.
(34) Stein, D.; Kruithof, M.; Dekker, C. *Phys. Rev. Lett.* **2004**, *93*, 035901.
(35) Corry, B.; Kuyucak, S.; Chung, S. H. *Biophys. J.* **2000**, *78*, 2364–2381.
(36) Pennathur, S.; Santiago, J. G. *Anal. Chem.* **2005**, *77*, 6782–6789.
(37) Schoch, R. B.; Lintel, H. V.; Renaud, P. *Phys. Fluids* **2005**, *17*, 100604.
(38) White, H. S.; Bund, A. *Langmuir* **2008**, *24*, 2212–2218.
(39) Ai, Y.; Zhang, M.; Joo, S. W.; Cheney, M. A.; Qian, S. *J. Phys. Chem. C* **2010**, *114*, 3883–3890.
(40) Cervera, J.; Schiedt, B.; Ramírez, P. *Europhys. Lett.* **2005**, *71*, 35–41.
(41) Qian, S.; Joo, S. W.; Ai, Y.; Cheney, M. A.; Hou, W. *J. Colloid Interface Sci.* **2009**, *329*, 376–383.
(42) Qian, S.; Joo, S. W. *Langmuir* **2008**, *24*, 4778–4784.
(43) Qian, S.; Joo, S. W.; Hou, W.; Zhao, X. *Langmuir* **2008**, *24*, 5332–5340.
(44) Qian, S.; Wang, A. H.; Afonien, J. K. *J. Colloid Interface Sci.* **2006**, *303*, 579–592.
(45) Yalcin, S. E.; Lee, S. Y.; Joo, S. W.; Baysal, O.; Qian, S. *J. Phys. Chem. B* **2010**, *114*, 4082–4093.
(46) Lund, M.; Jönsson, B.; Woodward, C. E. *J. Chem. Phys.* **2007**, *126*, 225103.
(47) Kesvatera, T.; Jönsson, B.; Thulin, E; Linse, S. *J. Mol. Biol.* **1996**, *259*, 828–839.
(48) Smith, P. E.; Brunne, R.; Mark, A. E.; van Gunsteren, W. F. *J. Phys. Chem.* **1993**, *97*, 2009–2014.
(49) Alexov, E. G.; Gunner, M. R. *Biophys. J.* **1997**, *5*, 2075–2093.
(50) Demchuk, E.; Wade, C. *J. Phys. Chem.* **1996**, *100*, 17373–17387.
(51) Kesvatera, T.; Jönsson, B.; Thulin, E.; Linse, S. *Proteins* **1999**, *37*, 106–115.
(52) Wei, C.; Bard, A. J.; Feldberg, S. W. *Anal. Chem.* **1997**, *69*, 4627–4633.